Mutational analysis of the catalytic centre of the *Citrobacter freundii* AmpD *N*-acetylmuramyl-ʟ-alanine amidase

Catherine GÉNÉREUX*, Dominique DEHARENG*, Bart DEVREESE†, Jozef VAN BEEUMEN†, Jean-Marie FRÈRE* and Bernard JORIS*[1]

*Center for Protein Engineering, Liège University, Institut de Chimie, B6, Sart-Tilman, B-4000 Liège, Belgium, and †Laboratorium voor Eiwitbiochemie en Eiwitengineering, Universiteit-Gent, K.L. Ledeganckstraat, 35, B-9000 Gent, Belgium

Citrobacter freundii AmpD is an intracellular 1,6-anhydro-*N*-acetylmuramyl-ʟ-alanine amidase involved in both peptidoglycan recycling and β-lactamase induction. AmpD exhibits a strict specificity for 1,6-anhydromuropeptides and requires zinc for enzymic activity. The AmpD three-dimensional structure exhibits a fold similar to that of another Zn^{2+} *N*-acetylmuramyl-ʟ-alanine amidase, the T7 lysozyme, and these two enzymes define a new family of Zn-amidases which can be related to the eukaryotic PGRP (peptidoglycan-recognition protein) domains. In an attempt to assign the different zinc ligands and to probe the catalytic mechanism of AmpD amidase, molecular modelling based on the NMR structure and site-directed mutagenesis were performed. Mutation of the two residues presumed to act as zinc ligands into alanine (H34A and D164A) yielded inactive proteins which had also lost their ability to bind zinc. By contrast, the active H154N mutant retained the capacity to bind the metal ion. Three other residues which could be involved in the AmpD catalytic mech-

anism have been mutated (Y63F, E116A, K162H and K162Q). The E116A mutant was inactive, but on the basis of the molecular modelling this residue is not directly involved in the catalytic mechanism, but rather in the binding of the zinc by contributing to the correct orientation of His-34. The K162H and K162Q mutants retained very low activity (0.7 and 0.2 % of the wild-type activity respectively), whereas the Y63F mutant showed 16 % of the wild-type activity. These three latter mutants exhibited a good affinity for Zn ions and the substituted residues are probably involved in the binding of the substrate. We also describe a new method for generating the *N*-acetylglucosaminyl-1,6-an-hydro-*N*-acetylmuramyl-tripeptide AmpD substrate from purified peptidoglycan by the combined action of two hydrolytic enzymes.

Key words: AmpD, β-lactamase induction, muropeptide, peptidoglycan recycling, site-directed mutagenesis, zinc amidase.

INTRODUCTION

In the bacterial cell wall, the peptidoglycan or murein is a rigid macropolymer surrounding the cytoplasmic membrane. Its remarkable rigidity allows eubacteria to resist their high intracellular osmotic pressure and confers to these micro-organisms their specific shape. The peptidoglycan is composed of glycan chains of alternating units of GlcNAc (*N*-acetylglucosamine) and MurNAc (*N*-acetylmuramic acid), which are cross-linked by short peptides. In Gram-negative bacteria the peptides are usually ʟ-alanyl-γ-D-glutamyl-meso-diaminopimelyl-D-alanine and are linked to the glycan via an amide bond between the MurNAc carboxyl group and the ʟ-Ala amino group of the tetrapeptide.

Cell growth as well as the separation of the daughter cells during cellular division requires a continuous remodelling of peptidoglycan achieved by specific hydrolases (autolytic enzymes), among which MurNAc-ʟ-Ala amidases (*N*-acetylmuramyl-ʟ-alanine amidases) specifically cleave the amide bond between the lactyl group of the MurNAc and the α-amino group of the peptide bridge ʟ-alanine.

In *Escherichia coli* and presumably most other Gram-negative bacteria, like *Citrobacter freundii* and *Enterobacter cloacae*, 40–50 % of the peptidoglycan is degraded at each generation [1–3] and 90 % of the degraded products are recycled. The major recycled compound resulting from the combined action of the periplasmic lytic transglycosylase and ʟ,D-carboxypeptidase

is GlcNAc-anhMurNAc-tripeptide (*N*-acetylglucosaminyl-1,6-anhydro-*N*-acetylmuramyl-tripeptide), which is transported in the cytoplasm by the AmpG permease [4,5]. It is then either directly cleaved by the cytoplasmic AmpD anhydroMurNAc ʟ-Ala amidase (anhydro-*N*-acetylmuramyl-ʟ-alanine amidase) or first converted into anhMurNAc-tripeptide (anhydro-*N*-acetylmuramyl-tripeptide) by a cytosolic β-*N*-acetylglucosaminidase [6] and subsequently hydrolysed by AmpD. Interestingly, AmpD has a strict specificity for 1,6-anhydro muropeptides and therefore does not hydrolyse the murein precursor molecules such as UDP-MurNAc-pentapeptide (UDP-*N*-acetylmuramyl-ʟ-alanyl-γ-D-glutamyl-meso-diaminopimelyl-D-alanyl-D-alanine) also present in the cytoplasm. Accordingly, AmpD does not interfere with peptidoglycan biosynthesis and controls the level of the recycled anhydromuropeptides in the cytoplasm. In Gram-negative bacteria having an inducible AmpC β-lactamase, the induction mechanism is directly linked to the relative cytoplasmic levels of anhydro muropeptides and UDP-MurNAc-pentapeptide. Inactivation of the *ampD* gene leads to constitutive β-lactamase overproduction in *C. freundii* and *Enterobacter cloacae* [7,8]. The activity of the *C. freundii* AmpD amidase has been shown to be Zn^{2+}-dependent and its three-dimensional structure in solution has been established [9].

Based on the NMR structure of *C. freundii* AmpD [9], the amino acids predicted to be Zn^{2+} ligands of AmpD include His-34, His-154 and Asp-164. Tyr-63 and Lys-162 are also involved
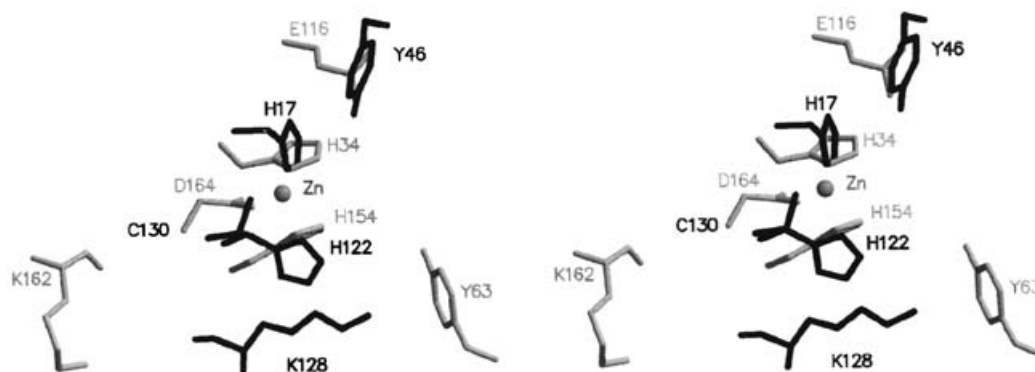
Figure 1   Stereo view of the superimposition of AmpD and T7 lysozyme with their zinc ligands

AmpD is shown in light grey and T7 lysozyme in black. The zinc ion is represented as a sphere.

in the catalytic mechanism (Figure 1). This is in accordance with another Zn^{2+} MurNAc-L-Ala amidase, the T7 lysozyme [10], whose structure has been solved by X-ray crystallography at 2.2 Å resolution and which exhibits a fold similar to that of AmpD, although the two proteins share only 20 % sequence identity.

A Blast search of sequence databases shows that AmpD homologues are found in wide variety of micro-organisms, ranging from viruses to Gram-negative (*Enterobacter*, *Salmonella*, *Pseudomonas*) and Gram-positive (*Bacillus*, *Staphylococcus*) bacteria, including the filamentous genera (*Streptomyces*). Moreover, sequence alignments showed similarities with some eukaryotic PGRP (peptidoglycan-recognition protein) domains, suggesting similar substrate-binding sites, including zinc-binding and other residues essential for hydrolytic activity [9,11–13]. In the present study, we constructed, by molecular mechanics (MM) and dynamics, the complexes between AmpD and its substrate (anhMurNAc-tripeptide) and between AmpD and the MurNAc-tripeptide. Simultaneously, we investigated the AmpD active site by site-directed mutagenesis.

MATERIALS AND METHODS

Plasmid constructions and mutagenesis

The wild-type *C. freundii ampD* gene was cloned into the expression vector pET-9a [14] by PCR [15] with primers D#1 (5′-TAACATATGTTGTTAGACGAGGGCTGGCTG-3′) and D#2 (5′-AATGGATCCTGTAAACAGCGTCATGTCATC-3′) and plasmid pCJ1 as a DNA template [5] and the source of the *C. freundii ampD* gene. Amplification yielded a DNA fragment containing the entire *ampD* coding sequence flanked on the 5′ and 3′ ends by the *Nde*I and *Bam*HI restriction sites, respectively. This PCR fragment was cloned into PCR-Script™ to give pCIP 251. The DNA sequence of the insert was checked for mutations by sequencing both strands according to standard procedures [16]. Next pCIP 251 was digested by *Nde*I and *Bam*HI restriction enzymes and ampD was cloned as an *Nde*I–*Bam*HI fragment into pET-9a (Novagen) to yield pCIP 252. In this construct, *ampD* is under the control of the T7 promoter and inducible by isopropyl β-D-thiogalactoside.

Production of the *ampD* gene in which the mutations had been introduced was carried out using the QuikChange™ site-directed mutagenesis kit (Stratagene) with pCIP 251 as a template for PCR reactions. Reactions conditions were 5 min at 95 °C, then 18 cycles of 30 s at 95 °C, 1 min at 65 °C and 7 min at 68 °C, followed by 3 min at 68 °C. After plasmid amplification, *E. coli*

DH5α cells were transformed by the PCR product and colonies were isolated on LB agar plates containing 100 μg/ml ampicillin. To ensure that the clones used for further work contained no mutations other than the intended ones, the mutated plasmid of one clone of each mutant was prepared by miniprep and the *ampD* variant was sequenced on both strands. The different *ampD* mutants carried by pCIP 251 derivatives were restricted with the *Nde*I/*Bam*HI enzymes and the excised fragments were cloned into *Nde*I/*Bam*HI-digested pET-9a to yield expression vectors pCIP 253–pCIP 260.

Expression in *E. coli* and purification of wild-type or mutant AmpD amidases

E. coli BL 21(DE3)pLysS cells harbouring pCIP derivatives carrying wild-type or mutant *ampD* genes (the sequences of the primers can be obtained from the corresponding author on request) were grown at 37 °C in LB medium supplemented with kanamycin (50 μg/ml) and chloramphenicol (30 μg/ml) as selection agents. The expression of the wild-type AmpD was induced by addition of isopropyl β-D-thiogalactoside (400 μM, final concentration) when the cell density reached a D_{600} value of 0.7. After 2 h of induction, the cells of a 5 l culture were harvested by centrifugation (8300 *g*, 15 min, 4 °C), washed with 150 mM NaCl and then resuspended in 20 mM phosphate buffer (pH 7.0) containing 1 mM dithiothreitol (buffer A). Cell lysis was achieved with the help of a cell disintegrator (basic Z model; Constant Systems, Warwick, U.K.) at 4 °C with a pressure of 28 kp.s.i. (193 200 kPa). Benzonase (5 units/l of culture) and Pefabloc (0.1 mg/ml, final concentration) were added to cell lysates. The insoluble material was removed by centrifugation at 20 000 *g* for 15 min at 4 °C. The supernatant was dialysed overnight against buffer A. After dialysis, the lysate was centrifuged at 20 000 *g* for 15 min at 4 °C, microfiltered on 0.7 and 0.45 μm Millipore filters and loaded on to a Q-Sepharose column (2.6 cm × 30 cm, 160 ml; Amersham Biosciences, Uppsala, Sweden) equilibrated in buffer A. The column was eluted with a linear NaCl gradient (720 ml) from 0 to 1 M. The peak fractions containing the AmpD amidase were pooled, concentrated to 10 ml by ultrafiltration on 5000 Da-cutoff Amicon membranes and applied to a molecular sieve column of Sephacryl S100 HR (2.6 cm × 95 cm, 500 ml; Amersham Biosciences) equilibrated in buffer A. The fractions containing the amidase were collected and concentrated. After addition of 1.6 M $(NH_4)_2SO_4$, the enzyme was applied to a Source 15 ISO column (1.6 cm × 10 cm, 20 ml; Amersham Biosciences).

The AmpD enzyme was eluted with a linear gradient from 1.5 to 0 M $(NH_4)_2SO_4$. The fractions containing AmpD were collected and dialysed against 50 mM sodium phosphate buffer, pH 7.0, and concentrated by ultrafiltration. After addition of NaN_3 (1 mM, final concentration), the enzyme was stored at 4 °C. The mutant AmpD proteins were overproduced and purified as described above except that the third step was not performed. The protein content of the column fractions was monitored by SDS/PAGE. The AmpD concentration was determined by measuring the absorbance of the solution at 280 nm and using a molecular absorption coefficient of 31960 $M^{-1} \cdot cm^{-1}$ calculated with the ProtParam tool (http://www.expasy.ch).

MS

The purity and molecular masses of the wild-type protein and the AmpD substrate were determined with the help of an electrospray mass spectrometer as described previously [17].

Metal content analysis

An aliquot (1 ml) of a 1 mg/ml solution (48 μM) of wild-type or mutant AmpD enzyme was dialysed overnight against 250 ml of doubly distilled water containing 10 mM Hepes, pH 7.0, at 4 °C. The zinc content of the enzyme was measured by ICPMS (inductively coupled plasma MS) with the help of a Fison spectrometer (Fison VG Plasmaquad PQII + ; Fison, Manchester, U.K.). The dialysis buffer contained an average of $\leqslant 0.15$ μM Zn^{2+}.

Preparation of the GlcNAc-anhMurNAc-tripeptide

The AmpD substrate was prepared from purified *Bacillus megaterium* peptidoglycan devoid of teichoic acid [18]. Peptidoglycan (30 mg) in 3 ml of 100 mM ammonium acetate buffer, pH 6.5, was incubated overnight with purified bacteriophage λ lysozyme [19] (3 %, w/v). The cleavage of the polysaccharidic chain was followed by cleavage of the peptide bridge by the purified *Streptomyces albus G* D,D-carboxypeptidase [20] (3 %, w/v) in the same buffer adjusted to pH 8.3 and supplemented with 5 mM $MgCl_2$. After purification by reversed-phase HPLC the molecular mass of the substrate (GlcNAc-anhMurNAc-tripeptide; 851.6 Da) was determined by MS as described above.

Assay of amidase activity

Amidase activity was estimated by incubating the GlcNAc-anhMurNAc-tripeptide substrate with wild-type or mutant AmpD. The assays were carried out in 50 mM sodium phosphate buffer, pH 7, at 30 °C with substrate concentrations ranging from 18 to 240 μM and enzyme concentrations from 15 nM to 40 μM. The reactions were stopped by a 2 min contact with boiling water. Reaction products were separated and quantified on a C_{18} reversed-phase HPLC column (Symmetry Shield RP_{18} 5 μm, 3.9 mm × 150 mm; Waters) on a Waters Alliance 2690 System. The column was equilibrated with 0.02 % trifluoroacetic acid in water and eluted with a linear acetonitrile gradient from 3 to 12 % over 13 min with a flow rate of 1 ml/min.

Assay of the influence of metalloprotease inhibitors and bivalent metal cations on AmpD activity

The purified wild-type AmpD (400 nM) in buffer A was incubated with metal chelators such as EDTA (5 μM), dipicolinic acid (5 μM), 1,10-phenanthroline (5 μM), mercaptoacetic acid (1 mM), mercaptopropionic acid (1 mM) and thiomandelic acid (1 mM) for 30 min at 30 °C and the residual activity was estimated as described above (substrate and enzyme final concentrations of 180 μM and 80 nM, respectively). The recovery of AmpD activity was assayed on addition of bivalent metal cations ($ZnSO_4$, $CuSO_4$, $CoSO_4$, $NiSO_4$, $CdSO_4$ and $MnSO_4$, at final concentrations of 100 μM).

Search for AmpD inhibitors

Potential inhibitors of AmpD were 1,6-anhydro-β-D-glucopyranose (100 μM; Acros Organics), 2-bromomethyl-1,3-dioxolane (1 M; Acros Organics), L-Ala-paranitroanilide (5 mM; Bachem), D-Ala-paranitroanilide (5 mM; Bachem), H-Gly-paranitroanilide (500 μM; Bachem), acetylmuramyl-L-Ala-D-Glu-NH$_2$ (0.1125–0.9 mM; Bachem) and anhydro-GlcNAc. The latter was synthesized as follows: GlcNAc (2 g, 9 mmol; Sigma) was dissolved in dry pyridine (10 ml) and cooled to 0 °C. A solution of toluene-*p*-sulphonyl chloride (2.4 g, 12.6 mmol; Acros Organics) in 5 ml of dry pyridine was added dropwise. After additional stirring for 3 h at 0 °C, TLC analysis (dichloromethane/methanol, 4:1, v/v) indicated conversion of the starting material into a predominantly tosylated form. The stirred reaction mixture was adjusted to pH 10 by the addition of an aqueous solution of NaOH (1 M) and kept at 0 °C for 1 h at pH 10. TLC analysis (dichloromethane/methanol, 3:1, v/v) of the reaction showed conversion of tosylated compound into 1,6-anhydro-GlcNAc. The solution was neutralized by addition of 3 M HCl and concentrated *in vacuo*, diluted in pyridine (25 ml) and evaporated again. The last step was repeated twice. To remove the traces of pyridine, the residue was solubilized in dichloromethane (30 ml), washed with water (20 ml), evaporated and finally dissolved in water. The analysis of the solubilized compound by MS showed that the 1,6-anhydroGlcNAc was the major compound of the mixture.

Thermal denaturation of wild-type and mutant AmpD

Intrinsic tryptophan fluorescence was monitored using an SLM-Aminco 8100/2 spectrometer (Spectronic Instruments, Rochester, NY, U.S.A.), with excitation and emission wavelengths of 285 and 339 nm, respectively. Bandwidths were 4 nm for excitation and 8 nm for emission. Protein concentration was 25 μg/ml. To monitor thermal denaturation of the wild-type or mutant AmpD enzymes, the fluorescence at 339 nm was recorded at constant heating rates of 1 °C/min from 20 to 90 °C. The temperature in the thermostat-controlled cuvette was monitored continuously with a differential thermometer. Intrinsic tryptophan fluorescence spectra of the native and denatured proteins were scanned between 300 and 400 nm with an excitation wavelength of 285 nm. The experimentally determined native fraction is given by eqn (1):

$$F_{\text{native}} = [S_{\text{mes}} - (U + zT)]/[(N + yT) - (U + zT)] \tag{1}$$

where S_{mes} was the signal measured by fluorescence and F_{native} is the native fraction. The terms $(N + yT)$ and $(U + zT)$ were necessary to account for the linear decreases of the intrinsic fluorescence of the native and denatured states of the protein (N and U, respectively) upon increasing the temperature.

Thermal denaturations were not reversible, so the T_m (melting temperature) values, which are the mid-transition points, have no thermodynamic meaning and are referred to as 'apparent T_m' in the text. T_m were determined in absence or presence of 100 μM $ZnCl_2$.

Molecular modelling

The start position of the complexes between the enzyme and both small molecules were built by manually docking the substrate in the cavity with the program Insight II (USA Biosym Technologies, San Diego, CA, U.S.A.; http://www.accelrys.com). Thereafter, the geometries of the complexes were optimized without any restraint at the MM level [21] with the Amber force field [22,23] and using the program Discover (USA Biosym Technologies; http://www.accelrys.com) running on an SGI Indy workstation. The Amber energy terms used for the minimization are the following:

$$E = \sum_b K_2 (b - b_0)^2 + \sum_\theta H_\theta (\theta - \theta_0)^2$$

$$+ \sum_\phi \frac{V_n}{2} [1 + \cos^2 (n\phi - \phi_0)] + \sum \varepsilon[(r^*/r)^{12} - 2(r^*/r)^6]$$

$$+ \sum q_i q_j / \varepsilon_{ij} r_{ij} + \sum \left[\frac{C_{ij}}{r_{ij}^{12}} - \frac{D_{ij}}{r_{ij}^{10}} \right] \tag{2}$$

The first three terms handle the internal co-ordinates of bonds, angles and dihedrals. The fourth and fifth account for the van der Waals and the electrostatic interactions. The final term is a hydrogen-bond term that augments the electrostatic description of the hydrogen bonds. The parameters used were those describing peptides or nucleotides [22,23].

Since the classical force field is not parameterized for describing bicyclo rings like the anhydro head, the geometry of the anhMurNAc-tripeptide and the MurNAc-tripeptide were optimized at the quantum chemistry semi-empirical AM1 level [24]. This was done to ensure that the starting geometry of the substrates was reliable. The program used was Gaussian98 (revision A6; Gaussian, Pittsburgh, PA, U.S.A.; http://www.gaussian.com) running on an eight-processor DEC-alpha 8400. As to the electrostatic terms for the non-bonded interactions of the MM field, the net charges used for the substrates were determined at the quantum chemistry level, at the restricted Hartree–Fock level [25] with the 6-31G basis set [26,27]. A dynamical study was performed with the program Discover. The geometry optimizations were performed without water, a dielectric constant of 2 was chosen and the threshold for convergence was taken to be the maximum force fixed at $0.02 \text{ kcal} \cdot \text{mol}^{-1} \cdot \text{Å}^{-1}$ (1 kcal = 4.184 kJ). In the dynamical calculations which considered a layer of about 1100 water molecules, the dielectric constant was taken as 1, the temperature was fixed at 300 K and the time of the simulation was 30 ps following a pre-equilibration step of 30 ps at 300 K.

RESULTS

Modelling (NMR results compared with MM results)

The structure obtained by NMR [9] was optimized at the MM level before docking and molecular dynamics (Table 1). It must be emphasized here that in both the NMR and the MM structures, the external His side chains in contact with the solvent, such as that of His-18, were considered as protonated, since the NMR experiments were performed at pH 5.5.

The MM distances between the zinc and either the His or Asp ligands are in better agreement with those observed in the crystal structures of other zinc hydrolases, for instance in entries 3TMN, 1LBU, 1C7K and 1G12 [28–31] of the Protein Data Bank (now maintained by the Research Collaboratory for Structural

Table 1   Distances between the zinc cation and its potential ligands in the AmpD structure

Bond	Distance (Å)	
	NMR	MM
Zn–N$_{\delta 1}$ (His-34)	2.23	2.33
Zn–N$_{\delta 1}$ (His-154)	2.23	2.40
Zn–O$_{\delta 1}$ (Asp-164)	2.27	2.02
Zn–O$_{\delta 2}$ (Asp-164)	2.12	2.05
Zn–O$_{\varepsilon 1}$ (Glu-116)	6.47	6.89
N$_{\varepsilon 2}$ (His-34)–O$_{\varepsilon 1}$ (Glu-116)	2.66	2.72

Bioinformatics; http://www.rcsb.org/pdb/index.html) in which the Zn–O(Asp) are always shorter than the Zn–N(His) distances. It appeared that the zinc could also be co-ordinated by the oxygen of the Asn-35 backbone.

Optimization of the complexes

The amidase substrate molecules have been subdivided into a head, a scissile bond and a tail (Figure 2). The head is either an N-acetyl-anhydromuramyl (Figure 2B) or an N-acetylmuramyl (Figure 2A) residue, the scissile bond is that cleaved by the AmpD amidase and the tail the tripeptide stem of the peptidoglycan. Two complexes with the anhydro head and two with the MurNAc head were built by docking the small molecule into the enzyme active site. The head was positioned inside the cleft and the oxygen of the scissile bond was oriented toward the zinc cation. The tail was oriented either towards Lys-162 [anhydroMurNAc_1 complex (Figure 3A) and MurNAc_1 complex], or towards Arg-22 and Asn-109 [anhydroMurNAc_2 complex (Figure 3B) and MurNAc_2 complex], both residues lying on the solvent-accessible surface of the enzyme. The results of the MM geometry optimizations of the four complexes are available on request and described below. Several hydrophobic residues are involved in the interactions with the head of the substrate in both types of complex: Pro-39, Val-72, Ile-67, Leu-51, Ile-56 and possibly also the neighbouring Pro-40, Ile-36 and Leu-38. However, we do not understand why the anhMurNAc-tripeptide behaves as a substrate while the MurNAc-tripeptide does not, since they both exhibit favourable interactions with the cavity. The difference could be due to the existence in MurNAc-tripeptide of two additional rotatable OH groups (the C_6 and C_1 hydroxyls), whose hydrogens decrease the influence of the oxygens. The interaction distances in optimized structures reflect a static situation. When the temperature effect is taken into account, the motions of these groups can most probably be a destabilizing factor.

Dynamical calculation results

The dynamics study was performed on solvated systems. The chosen optimized complexes were solvated in two steps. A first layer of 76 (for the anhydroMurNAc) or 63 (for the MurNAc) water molecules was created around the substrate, in the solvent-accessible area. The second layer is made up of 1057 (anhydroMurNAc) or 1033 (MurNAc) water molecules distributed around the whole complex. The water bath was provided by the Insight II program. A rough optimization of the solvent shell was performed until the maximum force on these molecules was lower than $1 \text{ kcal} \cdot \text{mol}^{-1} \cdot \text{Å}^{-1}$ and a first dynamical run was done at 300 K for 30 ps with a decreasing restraint from 1000 to $200 \text{ kcal} \cdot \text{mol}^{-1} \cdot \text{Å}^{-2}$ on all the water oxygens. No other restraints were imposed. The final dynamical run described below starts
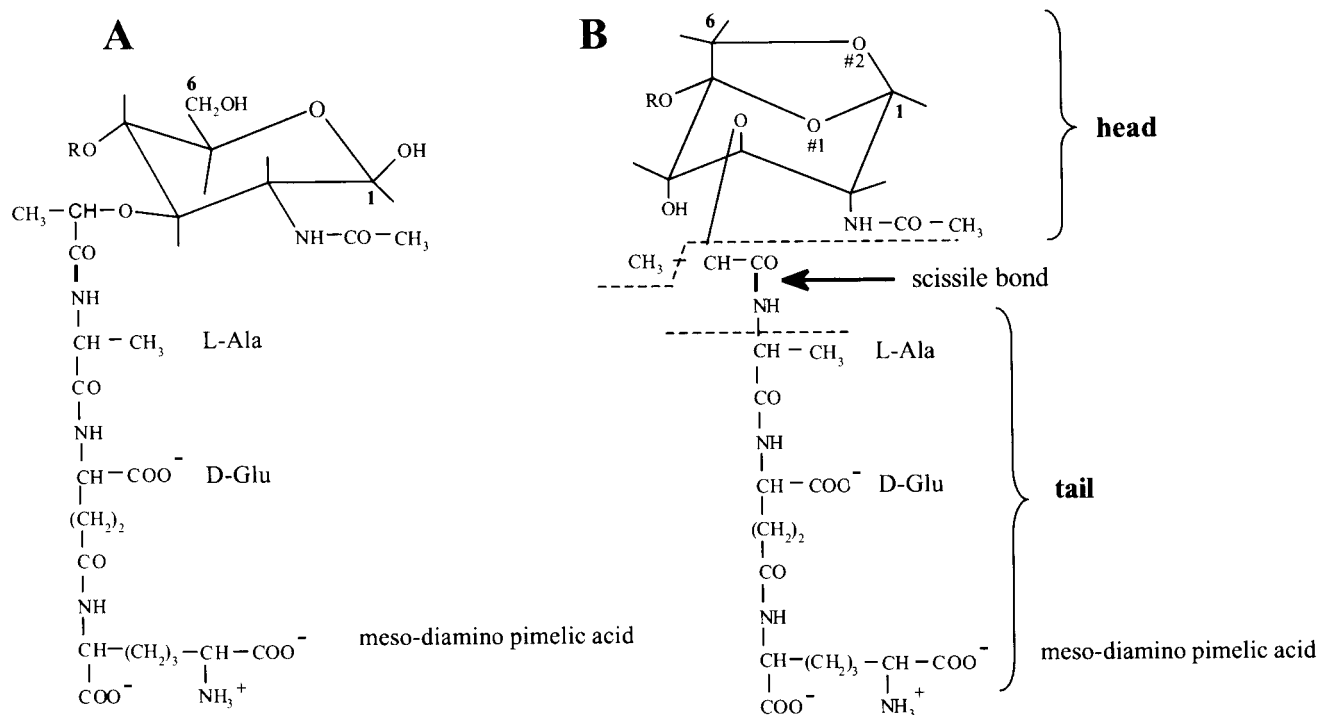
Figure 2   Structure of the MurNAc-tripeptide (A) and anhMurNAc-tripeptide (B) substrates

R = H or GlcNAc. In (**B**), the O#1 is defined as the anhydro oxygen and the O#2 as the pyrano oxygen.

from the solvated complex obtained in the first dynamical run for which the potential energy was the lowest. It also lasts 30 ps at 300 K. In order to avoid water evaporation during the process, a restraint of $200\ \mathrm{kcal \cdot mol^{-1} \cdot \mathring{A}^{-2}}$ was maintained on the oxygens of the water molecules in the second layer.

Only one pair of complexes was at first considered, anhydro-MurNAc_1 and MurNAc_1. Then, in order to eliminate the proton on His-18, which interacts strongly with the anhydro head in the course of the dynamics (the smallest distance between the oxygens of the head and the His-18 side chain varies between 2.5 and 4.3 Å), two other complexes were considered in which His-18 was not protonated. These complexes, named anhydroMurNAc_3 and MurNAc_3, are built from anhydroMurNAc_1 and MurNAc_1. During the course of the dynamics, two water molecules, W1 and W2, are found to approach the zinc. The following conclusions derive from these results. If one considers that the interaction between $\mathrm{Zn^{2+}}$ and the negative head of Asp-164 is strong, one can relate short distances ($< 2\ \mathrm{\mathring{A}}$) and a small variation during the dynamics ($\approx 0.5\ \mathrm{\mathring{A}}$) with a strong interaction. Thus strong interactions are maintained during the dynamics between $\mathrm{Zn^{2+}}$ and (i) the oxygen of the scissile bond in all cases, (ii) the backbone oxygen of Asn-35 in three cases out of four, (iii) W1 in three cases and (iv) W2 in two cases.

However, His-34 and His-154 do not seem to remain good zinc ligands when the substrate is in the cavity. Moreover, the result is dependent on the dynamics considered. Favourable oxygen–hydrogen interactions between the substrate head and Ile-67, Leu-51 and Val-72 are found for anhydroMurNAc and MurNAc. More precisely, the distances O#1–$C_{\delta 1}$(Leu-51) for anhydroMurNAc and MurNAc and their ranges of variation are similar. By contrast, the distances O#2–C_{β}(Ile-67) and O#1–C_{γ}(Pro-39) are shorter for anhydroMurNAc than for MurNAc and their variations are also smaller, denoting a stronger interaction with the anhydro compound. Interestingly, the distance O#1–$C_{\delta 1}$(Ile-67) is shorter

for MurNAc but its variation is larger. As a general observation, all the distance variations are either similar, or larger in the case of MurNAc, as compared with the anhydro form. Furthermore, it appears that the C_6 and C_1 hydroxyl hydrogens of MurNAc undergo unfavourable interactions with Ile-67 and to a lesser extent with Leu-51. In the case of Val-72, the dynamics results for anhydroMurNAc_3 present two distinct phases, the first one corresponding to 0–16.2 ps where the considered distance is larger than 4 Å, and the second one extending from 16.4 to 30 ps during which this distance remains rather short. From all these results, it seems that the anhydro head is maintained more firmly in the cavity by the hydrophobic side chain residues than is MurNAc. One reasons for this could be the unfavourable role of the C_6 and C_1 hydroxyl hydrogens of MurNAc.

Structural localization of the different mutations

To map the active site of AmpD amidase, we introduced eight point mutations at six different amino acid positions in the AmpD polypeptide chain. Four of them will affect binding of the zinc ion: H34A, H154A, H154N and D164A. According to the three-dimensional models (Figure 3), Tyr-63 is pointing into the active site and might be involved in the catalytic mechanism, whereas Glu-116 could be in interaction with His-34 and could be important to adequately orient the imidazole ring of the histidine side chain to chelate the metal ion.

Overexpression and purification of wild-type and mutant AmpD amidases

After production of the different enzymes in *E. coli* BL21 (DE3)pLysS and their purification to protein homogeneity, a yield of 16 mg of wild-type AmpD/l of culture was obtained whereas those for AmpD mutants ranged from 8 mg/l for D164A to 36 mg/l
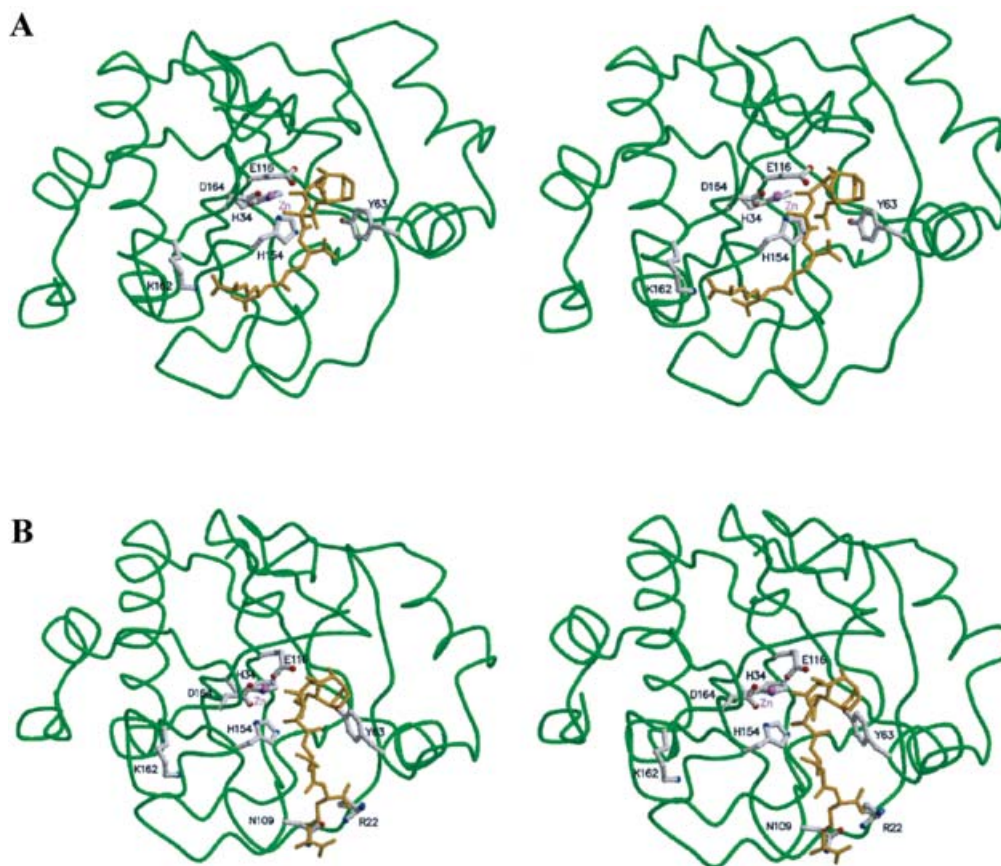
Figure 3   Stereo views of the two optimized models of the AmpD–substrate complexes

(**A**) AnhydroMurNAc_1 complex with the tail oriented towards Lys-162; (**B**) anhydroMurNAc_2 complex with the tail oriented towards Arg-22 and Asn-109. The polypeptide backbone is drawn in green. The zinc atom is depicted as a purple sphere with the side chains of the co-ordinating residues His-34, His-154, Asp-164 and the residues Tyr-63, Glu-116, Lys-162 drawn in bold. Red and blue spheres mark the oxygen and nitrogen atoms of these residues, respectively. The substrate 1,6-anhydroMurNAc-L-alanyl-γ-D-glutamyl-meso-diaminopimelic acid is drawn as an orange line.

for H34A. After the first two chromatographic steps, the enzymes were 95 % pure and the third step on the isopropyl Source column was performed to eliminate a contaminant protease and separate the wild-type AmpD isoforms. Indeed, on this hydrophobic column, the wild-type AmpD was eluted in two peaks exhibiting the same apparent molecular mass value on SDS/PAGE. The MS analysis showed that the two peaks were a mixture of the two polypeptide chains of 20847 Da (form I) and 20357 Da (form II). This difference between the two forms (490 Da) corresponds to deletion of the last four C-terminal residues of AmpD (Lys-Glu-Met-Thr; 489 Da). The molecular mass of form I matched that of the full-length wild-type AmpD (20847.17 Da). In the first and second peaks the ratios of form I/form II were 3:1 and 10:1, respectively. The NMR and kinetic studies revealed no difference between the enzymes in the two peaks (results not shown). For the AmpD mutants, the third chromatographic step was omitted.

Characterization of wild-type AmpD and inhibition of the enzyme activity

With no zinc ion added to the dialysis buffer (10 mM Hepes, pH 7.0, and a residual zinc concentration lower than 0.15 μM), the wild-type enzyme contained 0.7 ± 0.2 mol of zinc/mol of protein. After addition of 10 and 100 μM of ZnCl$_2$ to the dialysis buffer, the metal contents of AmpD enzyme increased to 1.3 and

3.7 mol/mol of protein, respectively. Inhibition of amidase activity by metal chelators was carried out by incubating the wild-type enzyme (final concentration, 80 nM) with EDTA, dipicolinic acid or 1,10-phenanthroline (final concentrations, 5 μM). In each case the enzyme was completely inhibited after 30 min and the activity was restored by addition of 100 μM (final concentration) ZnSO$_4$. Under the same conditions, CuSO$_4$, CoSO$_4$, NiSO$_4$, CdSO$_4$ and MnSO$_4$ did not restore even partial amidase activity.

The k_{cat}/K_m value of the hydrolysis of GlucNAc-anhMurNAc-tripeptide was 20000 ± 5000 M$^{-1} \cdot$ s^{-1}. Separate values for k_{cat} and K_m could not be obtained because the K_m value for this substrate is greater than 0.8 mM. Indeed, at this concentration substrate utilization was first order.

No inhibition of amidase activity was observed with compounds containing a 1,3-dioxolane ring as in the anhydroMurNAc, such as 1,6-anhydro-β-D-glucopyranose (final concentration, 100 μM), 2-bromomethyl-1,3-dioxolane (1 M) and anhydro-GlcNAc (this study). As suggested by molecular modelling, MurNAc-L-Ala-D-Gln was a competitive inhibitor with a K_i value of 190 ± 50 μM, estimated by incubating the enzyme with inhibitor concentrations ranging from 0.1 to 0.9 mM. Wild-type AmpD was also assayed for amidase activity by incubating the enzyme with L-Ala-paranitroanilide (5 mM), D-Ala-paranitroanilide (5 mM) and H-Gly-paranitroanilide (500 μM). Neither amidase activity nor inhibition was detected with these compounds.

Table 2 Properties of the AmpD mutants

The zinc ion content was determined by inductively coupled plasma MS in 10 mM Hepes at pH 7.0. The free zinc concentration was $\leqslant 0.15\ \mu$M. The kinetic parameters for the wild-type enzyme and the mutants were obtained in 20 mM phosphate at pH 7.0 and 30 °C. Relative k_{cat}/K_m is shown relative to the wild-type value. [E], enzyme concentration.

Enzyme	$[Zn^{2+}]/[E]$	k_{cat}/K_m (M$^{-1} \cdot$ s^{-1})	Relative k_{cat}/K_m (%)
Wild-type	0.7 ± 0.2	$20\,000 \pm 5000$	100
H34A	0.2 ± 0.1	< 1	< 0.2
Y63F	0.4 ± 0.1	3100 ± 300	16
E116A	0.3 ± 0.1	< 1	< 0.2
H154A	0.1 ± 0.05	2 ± 0.3	< 0.2
H154N	0.6 ± 0.2	$15\,000 \pm 3000$	76
K162H	0.5 ± 0.2	140 ± 14	0.7
K162Q	0.6 ± 0.2	33 ± 4	0.2
D164A	0.2 ± 0.1	< 1	< 0.2

Metal content of AmpD mutants

With no zinc added to the buffer, the zinc-ion content of the AmpD mutants is summarized in Table 2. Compared with the value of the wild-type enzyme (0.7 mol of zinc/mol of protein), the AmpD mutants fell into three categories: (i) the H154N, K162H and K162Q mutants exhibited zinc contents similar to that of wild-type AmpD; (ii) the Y63F and E116A mutants had slightly lower values in the range 0.3–0.4 mol of zinc/mol of protein and (iii) the H34A, H154A and D164A mutants did not bind more than 0.2 equivalents of zinc.
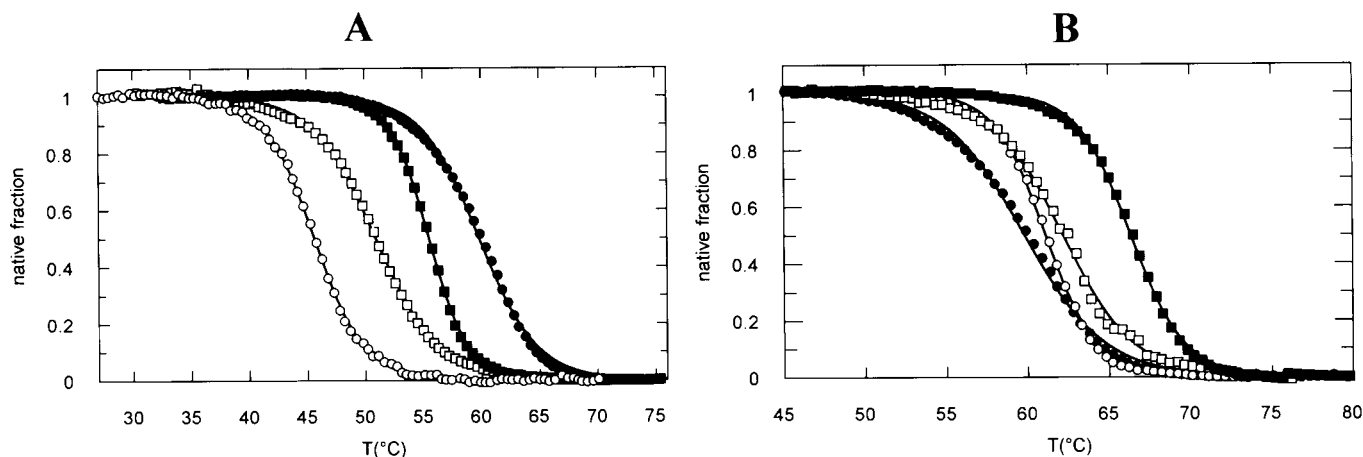
Thermal denaturation followed by fluorescence

AmpD has four tryptophan residues, which dominate the fluorescence spectrum, seven tyrosines and seven phenylalanines, which make small contributions to the overall intrinsic protein fluorescence. Using an excitation wavelength of 285 nm, the fluorescence emission spectra of the AmpD mutants were superimposable on to that of the wild-type enzyme (results not shown). As the subtle structural differences that might be expected could therefore not be detected by UV fluorescence, the thermal stability of the different enzymes was determined by the analysis of their thermal unfolding. A rigorous thermodynamic analysis of

Table 3 T_m values of wild-type and mutant AmpDs with and without ZnCl$_2$ (100 μM)

AmpD	T_m (°C)	$\Delta T_{m(WT-mutant)}$ (°C)	$\Delta T_{m(100\ \mu M\,Zn-0\ \mu M\,Zn)}$ (°C)
Wild-type (WT)	59.8	–	− 0.1
Wild-type + Zn^{2+}	59.7		
H34A	50.9	− 8.9	− 15.9
H34A + Zn^{2+}	35		
Y63F	61.1	+ 1.3	− 6.4
Y63F + Zn^{2+}	54.7		
E116A	66.3	+ 6.5	− 4.1
E116A + Zn^{2+}	62.2		
H154A	55.5	− 4.3	− 3.2
H154A + Zn^{2+}	52.3		
H154N	59.6	− 0.2	− 2.4
H154N + Zn^{2+}	57.2		
K162H	62.2	+ 2.4	− 6.1
K162H + Zn^{2+}	56.1		
K162Q	60	+ 0.2	− 1.5
K162Q + Zn^{2+}	58.5		
D164A	45.6	− 14.2	− 6.2
D164A + Zn^{2+}	39.4		

thermal unfolding curves from modified and wild-type AmpD was not possible due to the irreversibility of the phenomenon. However, thermal unfolding curves established by recording the decrease of the fluorescence at 339 nm induced by a temperature increase at a rate of 1 °C/min were used to determine the apparent T_m values (Table 3 and Figure 4).

Regarding their relative intrinsic stabilities against temperature, the most significant differences, when compared with the wild-type enzyme ($T_m = 59.8$ °C), were observed when zinc ligands were substituted with alanine [H34A, $\Delta T_{m(WT-mutant)} = -8.9$ °C; H154A, $\Delta T_{m(WT-mutant)} = -4.3$ °C; D164, $\Delta T_{m(WT-mutant)} = -14.2$ °C]. The H154N mutation, which modified the nature of the zinc ligand but retained its ability to form a complex with the metal ion, did not significantly modify the T_m value. The

Figure 4 Thermal denaturation followed by fluorescence

(**A**) Wild-type AmpD (●) and the H34A (□), H154A (■) and D164A (○) mutants. (**B**) Wild-type AmpD (●) and the Y63F (○), E116A (■) and K162H (□) mutants. K162Q and H154N mutants (not shown) followed the same profile as the wild type.

Y63F, E116A and K162H mutants were more stable than the wild-type enzyme, whereas the K162Q mutant was as stable as the native AmpD. The addition of an excess of $ZnCl_2$ (100 μM, final concentration) had no effect on the wild-type enzyme, but destabilized all the modified enzymes (Table 3). The maximum decrease in T_m was obtained for H34A mutant with a ΔT_m of $-15.9\,°C$ between 0 ($<0.15\,\mu$M) and 100 μM Zn^{2+}.

Kinetic studies

The catalytic efficiencies of the AmpD mutants against GlcNAc-anhMurNAc-tripeptide were compared with that of the wild-type enzyme at pH 7.0 ($k_{cat}/K_m = 20 \times 10^3\,M^{-1}\cdot s^{-1}$; Table 2). Substitutions of the residues of the zinc-binding site with an alanine (H34A, H154A and D164A) resulted in inactivation of the enzyme ($k_{cat}/K_m \leqslant 2\,M^{-1}\cdot s^{-1}$), which can be attributed to the loss of the active-site zinc ion (Table 2).

The zinc-dependence of the catalytic efficiencies of the wild-type enzyme and the H154A mutant was studied. For the wild-type AmpD, high Zn^{2+} concentrations up to 1 M did not modify the kinetic parameters whereas the k_{cat}/K_m of the H154A mutant increased to reach a maximum value of $13\,M^{-1}\cdot s^{-1}$.

On the other hand, the H154N substitution was designed to modify the nature of the zinc ligand while maintaining the capacity of the side chain to bind zinc. As postulated, the H154N mutant retained both its capacity to bind the zinc ion and good amidase activity.

The E116A mutant was totally inactive. The loss of its activity was attributed to its inability to bind zinc, although this residue does not interact directly with the metal ion.

Among the potential catalytic residues within the cleft which could be involved in the acid–base catalysis, Tyr-63 is well positioned and may have a critical role. By analogy with T7 lysozyme, Lys-162 was also considered, although it is not close to the active site. The results of site-directed mutagenesis support the idea that these two residues are important for amidase activity without affecting the ability of the mutants to bind the zinc ion (Table 2). The Y63F replacement was performed both to modify the H-bond-forming side chain of Tyr-63 and to assess the role of the tyrosine hydroxyl group in the acid–base catalysis. The Y63F mutation reduced the amidase activity by a factor 6. A part of this loss can be related to the level of zinc binding in the cavity. This seems to demonstrate that Tyr-63 is not involved in an acid–base mechanism. The increase in activation energy for the formation of the transition state complex [$\Delta(\Delta G^*)$] by replacing Tyr-63 with Phe was estimated to be $4.6\,kJ\cdot mol^{-1}$, using $\Delta(\Delta G^*) = -RT\ln[(k_{cat}/K_m)_{mutant}/(k_{cat}/K_m)_{WT}]$, indicating that Tyr-63 might supply a poor H-bond during the catalytic process. The replacement of Lys-162 with a His residue would confer a characteristic pH dependence to the kinetic parameters of the enzyme. Indeed, if the pK of the imidazole group is not perturbed by the protein environment, detectable effects should be recorded in a pH interval between 7 and 5.5. For the K162H mutant, a 4-fold decrease of the k_{cat}/K_m value was observed when the pH was decreased from 7 to 5.8. With the wild-type enzyme, the same result was obtained. The second mutation (K162Q) was designed to completely eliminate the proton-exchange ability and the net positive charge of the side chain. The K162H and K162Q mutants exhibited, respectively, 0.7 and 0.2% of the wild-type activity. The increases in activation energy [$\Delta(\Delta G^*)$] for the formation of the transition complex when replacing Lys-162 with His and Gln were estimated to be 12 and $16\,kJ\cdot mol^{-1}$ respectively, highlighting the importance of the Lys-162 side chain for the positioning of the ligand.

DISCUSSION

In the present work, we combined molecular dynamics and site-directed mutagenesis to study the catalytic mechanism of the AmpD amidase. The amidase activity was assayed with the GlcNAc-anhMurNAc-tripeptide, which is the compound generated by the autolytic system and transported into the cell by AmpG during the peptidoglycan-recycling process. In the cytoplasm of *E. coli* HfrH cells in which the *ampD* gene has been inactivated, the major accumulated compound is the anhMurNAc-tripeptide, generated by the action of the β-*N*-acetylglucosaminidase (NagZ) on the disaccharide anhMurNAc-tripeptide. Jacobs et al. [5] estimated that the K_m value was lower than 150 μM and that the k_{cat} value was $30 \pm 10\,s^{-1}$ for the anhMurNAc-tripeptide. By contrast, our results show that the K_m value for the disaccharide anhMurNAc-tripeptide is greater than 0.8 mM, yielding a k_{cat}/K_m value of $20000\,M^{-1}\cdot s^{-1}$. The comparison of the k_{cat}/K_m values for the two anhydro substrates suggests that, in the cytoplasm, the anhMurNAc-tripeptide is hydrolysed more rapidly than the GlcNAc-anhMurNAc-tripeptide. Consequently, the hydrolysis of the disaccharide anhMurNAc-tripeptide by NagZ might take place before the action of AmpD.

Purified wild-type AmpD amidase binds 1 mol of Zn^{2+}/mol of protein and the metal ion is required for amidase activity. In agreement with this interpretation, 1,10-phenanthroline or EDTA, strong Zn^{2+} chelators, inactivated the amidase activity, which was restored by adding Zn^{2+}. Clearly, the naturally occurring Zn^{2+} is essential for the amidase activity of AmpD. We showed that Cu^{2+}, Co^{2+}, Ni^{2+}, Cd^{2+} and Mn^{2+} could not activate the enzyme.

Based on the three-dimensional NMR structure of AmpD, the replacement of the three side chains (His-34, His-154 and Asp-164) involved in chelation of the zinc ion with alanine eliminated the amidase activity and the binding of the Zn^{2+} to the protein. The H154N substitution, which conserved the capacity of the side chain to bind the metal ion, produced a fully active mutant enzyme and confirmed the role of the three side chains cited above as the zinc ligands. In the bottom of the cavity, Glu-116 in close interaction with the imidazole ring of His-34 seems to be important for the good orientation of the histidine side chain to chelate the zinc ion. Indeed, the E116A mutant is completely inactive and has lost its zinc ion exactly as in the case of the substitutions of the zinc ligands by alanine. However, the large ΔT_m for this mutant ($\Delta T_m = +6.5\,°C$; Table 3) might suggest a substantial structural rearrangement and thus a different role for Glu-116.

The analysis of the docking of the anhMurNAc-tripeptide and the corresponding MurNAc compound into the AmpD catalytic cavity by molecular dynamics showed that the compounds could form stable complexes with the enzyme. It is not clear why AmpD is specific for the presence of the anhydro function borne by the MurNAc moiety of the substrate. Nevertheless, our results suggest that in the case of the MurNAc-tripeptide the orientation of the compound in the catalytic cavity might give rise to a catalytically unproductive complex. This hypothesis is consistent with the inhibition of AmpD amidase by MurNAc-L-Ala-D-Gln ($K_i = 190 \pm 50\,\mu$M). The results of the molecular dynamics seem to pinpoint an important mobility of the Zn^{2+} ligands during the formation of the Henri–Michaelis complex. This observation could be important for the catalytic mechanism. Two other residues, Tyr-63 and Lys-162, pinpointed by docking experiments, could be involved in the binding of the substrate in the catalytic cavity. In addition, the hydroxyl group of Tyr-63 remains close to the scissile peptide bond during the dynamics performed with the anhydro compound and could be involved in catalysis,
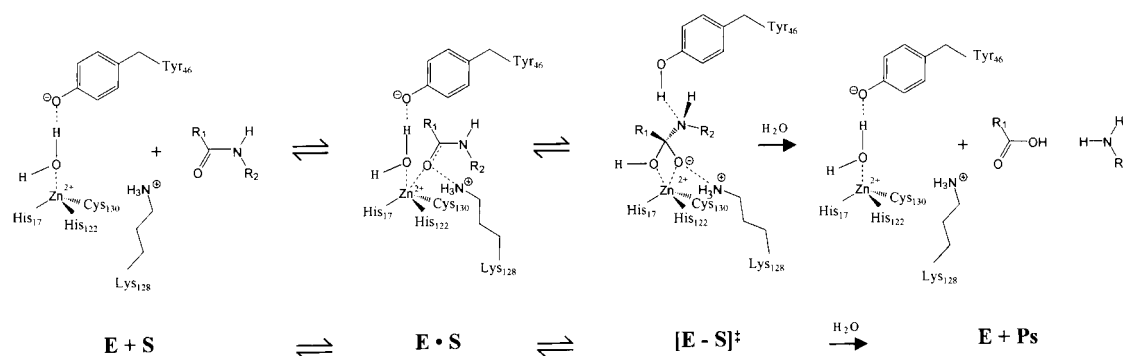
Scheme 1   Mechanism proposed in [10] for catalysis by T7 lysozyme

This mechanism is based on the experimental T7 lysozyme observation that the T7 Tyr-46 hydroxyl superimposes on to the Glu-270 of carboxypeptidase A. Note, however, that there is no direct experimental proof for the existence of a dissociated tyrosine phenol group. R_1, MurNAc; R_2, L-alanyl-γ-D-glutamyl-meso-diaminopimelyl-D-alanine; E $\cdot$ S, Michaelis–Menten complex; [E-S]‡, tetrahedral intermediate; Ps, products.

although in a minor way. The AmpD Y63F mutant remained 16% active compared with the wild-type enzyme, which might indicate that the Tyr-63 side chain is involved in substrate binding rather than catalysis. As predicted by molecular modelling, the Lys-162 side chain could be important for the binding of the substrate, since it interacts strongly with the carboxylate tail (Figure 3A) of the peptide. Both the K162H and K162Q mutants retained a very low activity, underlining the importance of a positive charge in this position. It was not possible to clearly test the possible effects of a positive His-162 side chain, since the enzymes precipitated at pH 5.5 and below. The superimposition of the equivalent zinc ligands in AmpD and T7 lysozyme (Figure 1) allows a comparison of their catalytic sites and suggests an important difference between the catalytic mechanisms of the two amidases. This difference is that the Lys-128 and Tyr-46 residues of T7 lysozyme (Scheme 1), which are suitably positioned to play the roles of acid–base catalysts in the reaction [10], are not present in the AmpD catalytic cavity. Tyr-63 in AmpD roughly points towards a position at the top of the cavity similar to that of Lys-128 in T7, but they are not oriented in the same way at all. Moreover, no residue occupying a position equivalent to that of Tyr-46 in the T7 amidase can be found in the AmpD catalytic site. In AmpD, Glu-116 cannot be equivalent to Tyr-46 in the T7 amidase. Indeed, Glu-116 is buried in the bottom of the cavity and too far away from the scissile amide bond, whereas Tyr-46 points directly into the T7 lysozyme catalytic cavity. Thus at this stage of our study, no amino acid side chain has been found in the AmpD active site that could play the role of a general base catalyst. For this reason, the AmpD catalytic mechanism remains obscure. Nevertheless, there is little doubt that the zinc ion acts as an electrophilic catalyst. The main catalytic role of the enzyme could be to enhance the peptide bond reactivity itself by polarizing the C=O bond and providing an sp3 character to the carbon and, consequently, decreasing the π delocalization on the peptide bond, leading to a larger N–C bond length and an easier pyramidalization or, in an equivalent way, a greater basicity of the nitrogen. Thus both the carbon and nitrogen of the peptide bond become more reactive towards water attack. This water molecule could be activated by the zinc ion itself or by another mechanism. This question remains open.

REFERENCES

1   Goodell, E. W. (1985) Recycling of murein by *Escherichia coli*. J. Bacteriol. **163**, 305–310

2   Goodell, E. W. and Schwarz, U. (1985) Release of cell wall peptides into culture medium by exponentially growing *Escherichia coli*. J. Bacteriol. **162**, 391–397

3   Park, J. T. (1993) Turnover and recycling of the murein sacculus in oligopeptide permease-negative strains of *Escherichia coli*: indirect evidence for an alternative permease system and for a monolayered sacculus. J. Bacteriol. **175**, 7–11

4   Jacobs, C., Huang, L. J., Bartowsky, E., Normark, S. and Park, J. T. (1994) Bacterial cell wall recycling provides cytosolic muropeptides as effectors for beta-lactamase induction. EMBO J. **13**, 4684–4694

5   Jacobs, C., Joris, B., Jamin, M., Klarsov, K., Van Beeumen, J., Mengin-Lecreulx, D., van Heijenoort, J., Park, J. T., Normark, S. and Frère, J. M. (1995) AmpD, essential for both beta-lactamase regulation and cell wall recycling, is a novel cytosolic N-acetylmuramyl-L-alanine amidase. Mol. Microbiol. **15**, 553–559

6   Votsch, W. and Templin, M. F. (2000) Characterization of a beta-N-acetylglucosaminidase of *Escherichia coli* and elucidation of its role in muropeptide recycling and beta-lactamase induction. J. Biol. Chem. **275**, 39032–39038

7   Lindberg, F., Lindquist, S. and Normark, S. (1987) Inactivation of the ampD gene causes semiconstitutive overproduction of the inducible *Citrobacter freundii* beta-lactamase. J. Bacteriol. **169**, 1923–1928

8   Jacobs, C. (1997) Pharmacia Biotech & Science Prize. 1997 Grand Prize Winner. Life in the balance: cell walls and antibiotic resistance. Science **278**, 1731–1732

9   Liepinsch, E., Généreux, C., Dehareng, D., Joris, B. and Otting, G. (2003) NMR structure of *Citrobacter freundii* AmpD, comparison with T7 lysozyme and homology with PGRP domains. J. Mol. Biol. **327**, 833–842

10 Cheng, X., Zhang, X., Pflugrath, J. W. and Studier, F. W. (1994) The structure of bacteriophage T7 lysozyme, a zinc amidase and an inhibitor of T7 RNA polymerase. Proc. Natl. Acad. Sci. U.S.A. **91**, 4034–4038

11 Kang, D., Liu, G., Lundstrom, A., Gelius, E. and Steiner, H. (1998) A peptidoglycan recognition protein in innate immunity conserved from insects to humans. Proc. Natl. Acad. Sci. U.S.A. **95**, 10078–10082

12 Liu, C., Xu, Z., Gupta, D. and Dziarski, R. (2001) Peptidoglycan recognition proteins: a novel family of four human innate immunity pattern recognition molecules. J. Biol. Chem. **276**, 34686–34694

13 Werner, T., Liu, G., Kang, D., Ekengren, S., Steiner, H. and Hultmark, D. (2000) A family of peptidoglycan recognition proteins in the fruit fly *Drosophila melanogaster*. Proc. Natl. Acad. Sci. U.S.A. **97**, 13772–13777

14 Studier, F. W. and Moffatt, B. A. (1986) Use of bacteriophage T7 RNA polymerase to direct selective high-level expression of cloned genes. J. Mol. Biol. **189**, 113–130

15 Innis, M. A. and Gelfond, D. H. (1990) Optimization of PCRs. In PCR Protocols (Innis, M. A., Gelfond, D. H., Snisky, J. J. and White, T. J., eds.), pp. 3–12, Academic Press, New York

16 Sanger, F., Nicklen, S. and Coulson, A. R. (1977) DNA sequencing with chain terminating inhibitors. Proc. Natl. Acad. Sci. U.S.A. **74**, 5463–5467

17 Cheggour, A., Fanuel, L., Duez, C., Joris, B., Bouillenne, F., Devreese, B., Van Driessche, G., Van Beeumen, J., Frère, J. M. and Goffin, C. (2000) The dppA gene of *Bacillus subtilis* encodes a new D-aminopeptidase. Mol. Microbiol. **38**, 504–513

18 Bricas, E., Ghuysen, J. M. and Dezelee, P. (1967) The cell wall peptidoglycan of *Bacillus megaterium* KM. I. Studies on the stereochemistry of α,α'-diaminopimelic acid. Biochemistry **6**, 2598–2607

19 Taylor, A. and Gorazdowska, M. (1974) Conversion of murein to non-reducing fragments by enzymes from phage lambda and Vi II lysates. Biochim. Biophys. Acta **342**, 133–136

20 Duez, C., Frère, J. M., Geurts, F., Ghuysen, J. M., Dierickx, L. and Delcambe, L. (1978) The exocellular DD-carboxypeptidase-endopeptidase from *Streptomyces albus G.* Purification and chemical properties. Biochem. J. **175**, 793–800

21 Burkert, U. and Allinger, N. L. (1982) Molecular Mechanics, American Chemical Society, Washington DC

22 Weiner, S. J. and Kollman, P. A. (1981) Amber: assisted model building with energy refining. a general program for modeling molecules and their interactions. J. Comp. Chem. **2**, 287–303

23 Weiner, S. J., Kollman, P. A., Nguyen, D. T. and Case, D. A. (1986) An all atom force field for simulations of proteins and nucleic acids. J. Comp. Chem. **7**, 230–252

24 Dewar, M. J. S., Zoebisch, E. G. and Healy, E. F. (1985) Development and use of quantum mechanical molecular models. 76. AM1: a new general purpose quantum mechanical molecular model. J. Am. Chem. Soc. **107**, 3902–3909

25 Jensen, F. (1998) in Introduction to Computational Chemistry, pp. 53–81, Wiley and Sons, Chichester

26 Dichtfield, R., Hehre, W. J. and Polple, J. A. (1971) Self-consistent molecular-orbital methods. IX. Extended Gaussian-type basis for molecular-orbital studies of organic molecules. J. Chem. Phys. **54**, 724–728

27 Hehre, W. J., Dichtfield, R. and Polple, J. A. (1972) Self-consistent molecular orbital methods. XII. Further extensions of Gaussian-type basis sets for use in molecular orbital studies of organic molecules. J. Chem. Phys. **56**, 2257–2261

28 Holden, H. M. and Matthews, B. W. (1988) The binding of L-valyl-L-tryptophan to crystalline thermolysin illustrates the mode of interaction of a product of peptide hydrolysis. J. Biol. Chem. **263**, 3256–3260

29 Dideberg, O., Charlier, P., Dive, G., Joris, B., Frère, J. M. and Ghuysen, J. M. (1982) Structure of a Zn^{2+}-containing D-alanyl-D-alanine-cleaving carboxypeptidase at 2.5 Å resolution. Nature (London) **299**, 469–470

30 Kurisu, G., Kai, Y. and Harada, S. (2000) Structure of the zinc-binding site in the crystal structure of a zinc endoprotease from *Streptomyces caespitosus* at 1 Å resolution. J. Inorg. Biochem. **82**, 225–228

31 Hori, T., Kumasaka, T., Yamamoto, M., Nonaka, N., Tanaka, N., Hashimoto, Y., Ueki, U. and Takio, K. (2001) Structure of a new 'aspzincin' metalloendopeptidase from *Grifola frondosa*: implications for the catalytic mechanism and substrate specificity based on several different crystal forms. Acta Crystallogr. D Biol. Crystallogr. **57**, 361–368